DOI: 10.13009/EUCASS2023-332
Aerospace Europe Conference 2023 – 10TH EUCASS – 9TH CEAS

Heterogeneous Combustion of AP/HTPB/RDX Propellants with Detailed Kinetics

P. Bernigaud [1†], *D. Davidenko* [1], *L. Catoire* [2]
[1] *DMPE, ONERA, Université Paris Saclay, 91120 Palaiseau, France*
[2] *Unité Chimie et Procédés (UCP), ENSTA Paris, Institut Polytechnique de Paris, 91120 Palaiseau, France*
pierre.bernigaud@onera.fr · dmitry.davidenko@onera.fr · laurent.catoire@ensta-paris.fr
[†]Corresponding author

Abstract

In this work, the effect of hexogen (RDX) inclusion in conventional ammonium perchlorate (AP) / hydroxyl-terminated polybutadiene (HTPB) composite propellants is investigated. To this end, a detailed gas-phase kinetic mechanism for AP/HTPB/RDX combustion is assembled and tested. The combustion of a single RDX particle surrounded by a layer of homogenized AP/HTPB binder is simulated with this kinetic model for various pressures and RDX particle sizes. A phenomenological description of the heterogeneous flame structure forming above the propellant is proposed. Two combustion modes are identified: hot and mild. Critical conditions for the combustion mode change are determined in terms of ambient pressure and RDX particle size.

1. Introduction

Composite propellants have been used for decades in civilian and military rocket systems. They are typically composed of a binder, which maintains the structural integrity of the propellant and provides combustible gases via its pyrolysis, associated with particulate components, which generate oxidizing gases or enhance energy release.

Ammonium perchlorate (AP) is a widely used oxidizer for solid propellants, mainly in association with a polymeric binder such as hydroxyl-terminated polybutadiene (HTPB). Reasons for their use are mostly the stability of this association, resulting in safe munitions, and the ability to control the propellant burning rate by modifying the distribution of AP particle sizes. These so-called AP/HTPB composite propellants have been studied extensively due to their prevalence in the rocket industry. When modelling AP/HTPB combustion, a possible hypothesis is to consider the AP particles to be small enough so that the overall combustion occurs in a premixed regime, ignoring any effects induced by the heterogeneous composition. The propellant is said to be homogenized and can be studied employing 1D approaches. Historically, detailed combustion models have been developed for this homogenized AP/HTPB system [1–3], and in recent years efforts have been directed toward modelling heterogeneous effects. As an example, Gross and Beckstead [3] performed 2D simulations of an AP particle surrounded by a layer of homogenized AP/HTPB binder, and demonstrated flame structures for such a heterogeneous system.

Next-generation propellants may include nitramine particles, such as hexogen (RDX), as a partial substitute for AP for some specific purposes. In particular, a decrease in the overall AP mass loading within the propellant reduces the amount of hydrochloric acid (HCl) produced by the combustion, hence resulting in an engine exhaust plume with reduced smoke signature [4]. Few experimental data exist on the combustion of so-called AP/HTPB/RDX propellants [4, 5], and many of the underlying processes driving their combustion are still unknown. To the authors' knowledge, no previous numerical investigation of the flame produced by such propellants has been conducted, mainly owing to difficulties in assembling a detailed kinetic model for the gaseous reactions between AP, HTPB and RDX.

In this work, the heterogeneous combustion of a AP/HTPB/RDX propellant is studied with detailed kinetics, employing the methodology previously used by Gross and Beckstead [3] for conventional AP/HTPB propellants. As a first step, leveraging previous work on pure AP combustion [6], a detailed kinetic model for the AP/HTPB/RDX system is assembled, and its ability to reproduce the combustion of pure AP, homogenized AP/HTPB, and pure RDX is demonstrated. The numerical method employed to compute the heterogeneous combustion of a composite propellant is described. Flame structures above AP and RDX particles surrounded by a layer of homogenized AP/HTPB binder are compared. A phenomenological description of the flame is proposed, and the influence on the combustion of relevant parameters (ambient pressure, RDX particle size) is highlighted.

DOI: 10.13009/EUCASS2023-332

2. AP/HTPB/RDX Combustion Model

2.1 Gas-Phase Kinetics

A necessary first step toward modelling AP/HTPB/RDX heterogeneous combustion consists in developing a chemical kinetic mechanism describing the gas-phase reactions between the various species produced by the decomposition of the ingredients. This mechanism must represent the combustion of each pure ingredient and the interactions between their respective gaseous products. Detailed combustion modelling of pure PA, homogenized AP/HTPB, and pure RDX can be found in the literature, but no example exists for a three-component system. An incremental methodology is used to develop such a model, starting from previous work on pure AP combustion (see Bernigaud et al. [6]). In this mechanism, the chemistry for AP-specific molecules (ex: $HClO_4$) is represented by sub-mechanisms from the historical AP model of Ermolin et al. [7] and the later of Meynet [8]. The main novelty introduced in this AP model is the use of recent advances from the chemical kinetics community to improve and validate the fundamental sub-mechanisms. For example, the ammonia combustion mechanism of Shrestha et al. [9] has been included to more finely represent the oxidation of NH_3, which is a major decomposition product of pure AP. In addition to the validation cases conventionally employed within the solid propellant community, the proposed AP mechanism was further validated against combustion experiments involving simple reactive systems of interest, such as laminar flame speed or ignition delay measurements. These test cases have highlighted fundamental deficiencies in previous reference mechanisms from the literature, demonstrating the importance of thorough validation of combustion models.

Starting from this solid base for pure AP combustion, the next development step consists in including the reactions specific to the AP/HTPB system. HTPB is a polymer composed primarily of butadiene monomers C_4H_6. In order to model the combustion of HTPB, sub-mechanisms are added for the oxidation of C_1, C_2 and C_4 species. These reactions come from a reduced version of the larger mechanism from Laskin et al. [10] for C_4H_6 oxidation. Finally, to model the interactions between the gaseous combustion products of AP and HTPB, bridge reactions between carbonated and chlorinated species are included. These reactions originate from the historical AP/HTPB mechanisms of Korobeinichev et al. [1], Jeppson et al. [2] and from the more recent work of Pelucchi et al. [11] on chlorine chemistry at high temperature. Following the methodology used for the first step, the mechanism is validated on usual experiments for the AP/HTPB system (regression rate, surface temperature) as well as on fundamental combustion experiments.

Finally, a specific sub-mechanism for the RDX combustion is included in the model from the historical model from Prasad et al. [12]. The complete AP/HTPB/RDX kinetic mechanism contains 77 species and 485 reactions.

2.2 Validation

The capability of the kinetic mechanism to model the combustion of the considered ingredients (pure AP, homogenized AP/HTPB, pure RDX) is presented. To this end, coupled flame / solid simulations are performed. This specific approach is widely used within the solid propellant combustion community to validate combustion models for specific ingredients. The method is first described and then applied to reproduce experimental data on the AP, AP/HTPB and RDX combustion.

2.2.1 Coupled 1D Numerical Model

Calculations are performed in a coupled approach with the condensed phase. A diagram of the simulated case is presented in Figure 1, showing schematically the temperature profile within the computational domain and phase transformation.

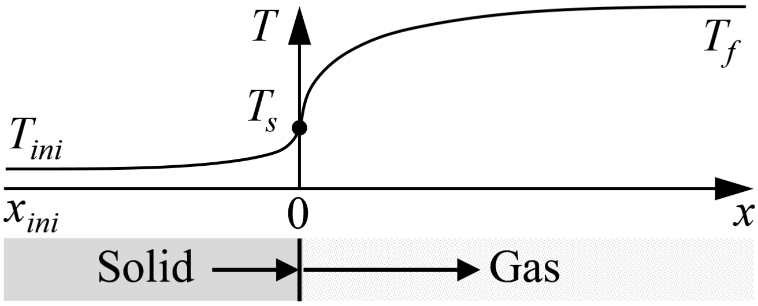

Figure 1: Schematic representation of the temperature profile and phase transformation in a coupled combustion simulation.

DOI: 10.13009/EUCASS2023-332

The gas and condensed phases are considered to be separated by a planar and infinitely thin interface. The heat equation is solved in the condensed phase, while usual equations for reactive flows are formulated in the gas-phase. The two phases are coupled at the interface via balance conditions for mass and energy fluxes. The combustion process is assumed to be one-dimensional and steady-state in the reference frame attached to the interface. For the sake of conciseness, the numerical procedure employed is not presented here. Extensive description can be found elsewhere (see Rahman et al. [13]).

A description of the chemical processes occurring within the solid energetic material is required to perform these calculations. The condensed-phase decomposition model consists of several global reaction steps describing the transformation of the solid ingredient into gaseous species. For pure AP, this decomposition model has been detailed in the previous work [6]. The coupled model permits to determine the regression rate of each ingredient at a given initial temperature and ambient pressure.

2.2.2 Coupled 1D Results

The combustion model is validated against experimental data on the regression rate for each of the considered ingredients. One of the main criteria for validating an ingredient-specific combustion model is its ability to reproduce the evolution of the regression rate as a function of pressure. These curves are shown in Figure 2 for pure AP, homogenized AP/HTPB, and pure RDX.

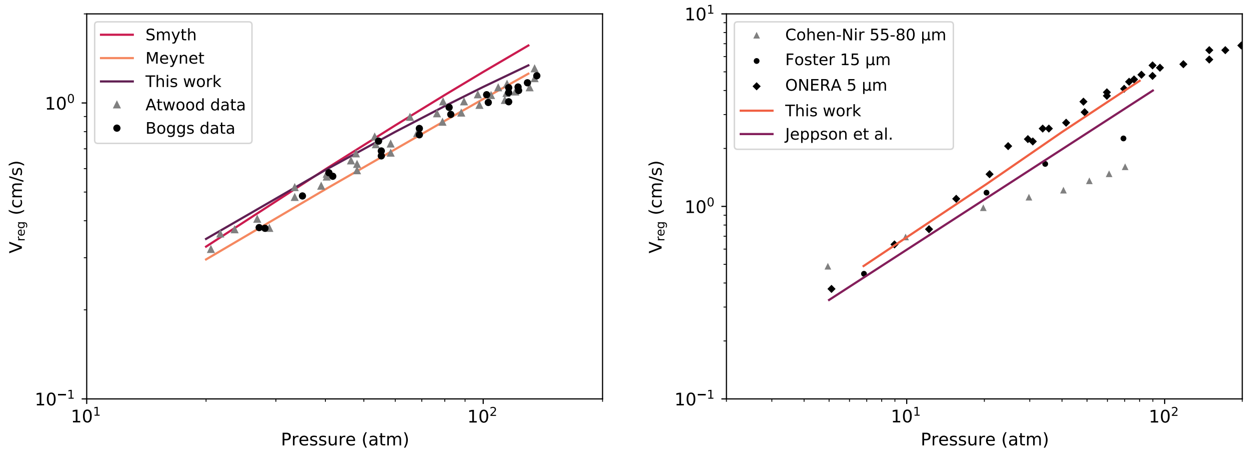

(a) Pure AP with experimental data [14,15] and reference models of Smyth [16] and Meynet [8].

(b) AP(80%)/HTPB with experimental data [17–19] and reference model of Jeppson et al. [2].

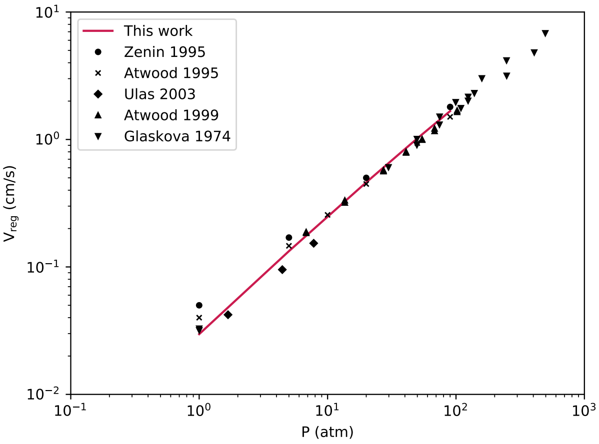

(c) Pure RDX with experimental data [15,20–23].

Figure 2: Evolution of the regression rate versus pressure for the considered ingredients, computed in a coupled 1D flame / solid approach. Initial temperature 298 K for all the ingredients.

DOI: 10.13009/EUCASS2023-332

In the case of pure AP combustion, Figure 2a, the experimental data suggest the pressure exponent of the law $V_{\text{reg}} = aP^n$ should be decreasing with increasing pressure. This experimental trend is captured by the present model, but not by the reference models of Smyth [16] and Meynet [8], which produce a straight line in this logarithmic scale plot.

For the case of a homogenized AP/HTPB propellant containing 80% AP by mass, Figure 2b, the historical model of Jeppson et al. [2] also provides reasonably satisfying results. The ingredient decomposition models describe the phenomenology of the underlying processes and are usually designed for use with a particular gas-phase mechanism. Hence, multiple variants of gas-phase kinetics and condensed-phase decomposition models can provide satisfactory results, the latter being generally tailored to this end.

One can also consider the effect of AP particle size on the AP/HTPB regression rate regarding the experimental data shown in this plot. For a given pressure, it increases with decreasing particle size, and this effect becomes more significant as the pressure grows up. In these coupled 1D simulations, the AP particles are considered to be infinitely small and perfectly mixed with the binder. Hence, the regression rate predicted follows the experimental data points for finer granulometry.

Finally, the evolution of the regression rate with pressure is shown in Figure 2c for pure RDX. Once again, good agreement is obtained with the experimental data. In the end, the proposed combustion model appears to reproduce the regression of all the considered ingredients. It mainly indicates that accurate modelling of the combustion processes occurring near the ingredient surface is achieved.

To further validate the combustion chemistry, one can try to replicate available experimental species profiles within the flame. These curves are presented in Figure 3 for pure AP and pure RDX. For both ingredients, the agreement is considered reasonable, even though a discrepancy is observed for the H_2O profile within the RDX flame. It is to be noted that very few data of this type exist in the literature, mainly owing to the practical difficulty of such measurements. The community would greatly benefit from the acquisition of more experimental results that would expand the validation dataset for such combustion models.

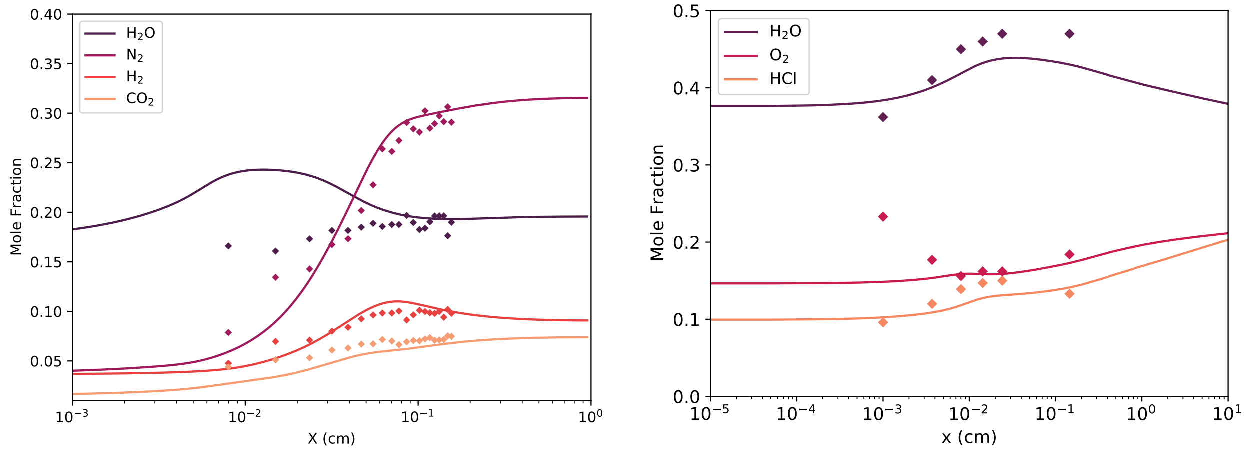

(a) Pure RDX, at initial temperature of 298 K. Pressure 1 atm. Symbols: experiment [24].

(b) Pure AP, at initial temperature of 533 K. Pressure 0.6 atm. Symbols: experiment [7].

Figure 3: Species profiles within the RDX (left) and AP (right) flames, computed in a coupled 1D flame/solid approach.

Ultimately, the proposed AP/HTPB/RDX model can represent the combustion of pure AP, homogenized AP/HTPB, and pure RDX. Each energetic material has specific chemistry, and the proposed mechanism seems to be capable of capturing the distinctive features of the combustion of each ingredient. Further work could be considered to improve the model, such as experimental characterization of the flame produced by an AP/RDX sandwich, to refine the interactions between these two ingredients. Nevertheless, the model performance shown is sufficient to explore numerically the interactions occurring during the heterogeneous combustion of these ingredients.

3. 2D Numerical Model

The objective is now to apply the AP/HTPB/RDX combustion model to the case of heterogeneous solid propellant. To this end, a dedicated Direct Numerical Simulation (DNS) solver called μSCOP (Microscale Simulation of COmposite Propellants) has been developed. It simulates the combustion of an isolated oxidizer particle (AP or RDX) surrounded by a layer of homogenized AP/HTPB binder. This configuration is represented in the numerical domain as a cylinder of oxidizer surrounded by an annulus of binder. A diagram of the computational case is presented in Figure 4.

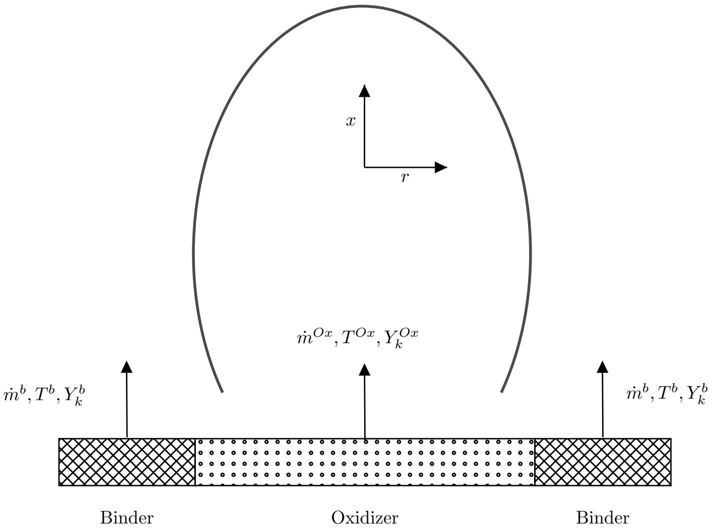

Figure 4: Diagram of the computational domain for the μSCOP code.

The conservation equations are solved for the gas-phase under the low Mach number hypothesis. Conservation of mass and momentum are written as:

$$\frac{\partial \rho}{\partial t} + \nabla (\rho \mathbf{u}) = 0 \tag{1}$$

$$\frac{\partial (\rho \mathbf{u})}{\partial t} + \nabla (\rho \mathbf{u} \otimes \mathbf{u}) = -\nabla p + \nabla \mathbf{\Sigma} \tag{2}$$

where ρ is the gas bulk density, $\mathbf{u}$ is the velocity vector, p is the hydrodynamic pressure, and $\mathbf{\Sigma}$ is the viscous stress tensor. For a gas of temperature T and composed of N_s chemical species with mass fractions Y_k, $k \in [1, N_s]$, conservation equations for energy and species masses are expressed as:

$$\frac{\partial (\rho h)}{\partial t} + \nabla (\rho h \mathbf{u}) = \nabla (\lambda \nabla T) - \sum_{k=1}^{N_s} \nabla (\rho h_k Y_k \mathbf{V_k}) \tag{3}$$

$$\frac{\partial (\rho Y_k)}{\partial t} + \nabla (\rho Y_k \mathbf{u}) = -\nabla (\rho Y_k \mathbf{V_k}) + \dot{m}_k \tag{4}$$

where h is the mass-specific enthalpy and λ is the thermal conductivity of the gas mixture; h_k is the mass-specific enthalpy, $\mathbf{V_k}$ is the diffusion velocity, and $\dot{m}_k$ is the mass production rate of species k. The diffusion of chemical species is modelled employing the generalized Fick law. The transport properties are computed via the EGLib library [25], and chemical kinetics via the CHEMKIN library [26].

The Equations (1)-(4) are discretized in space applying the finite volume method employing cylindrical coordinates in the 2D axisymmetric configuration. Looking for a steady-state solution, time derivatives are approximated via the implicit Euler scheme, ensuring intrinsic stability and allowing the use of large time steps. The overall system of discretized equations is solved employing a segregated method: Equations (3) and (4) are solved conjointly; the velocity field is then updated solving Equations (1) and (2) via the projection method [27]. The non-linear systems are efficiently solved employing a Newton-Krylov method provided by the PETSc library [28].

The solved problem is closed with appropriate boundary conditions. Symmetry conditions are imposed at the inner and outter radial boundaries. The outflow boundary uses a zero-gradient Von Neumann condition. The inlet boundary condition should take into account the heterogeneities introduced by the different ingredients, and model the response of the condensed phase to the heat flux from the flame. A straightforward solution would be to solve the heat equation in the condensed phase, as performed previously in the coupled 1D simulations. However, in the present study, only the flame is simulated and the condensed-phase behaviour is modelled as an inlet boundary condition. Following the approach previously taken by Gross and Beckstead [3], the state of the injected gas (mass flow $\dot{m}$, temperature T_s) depends on the heat flux Q transmitted via conduction from the flame to the condensed-phase surface :

DOI: 10.13009/EUCASS2023-332

$$Q = \lambda \frac{\partial T}{\partial x}\bigg|_{x=0} \tag{5}$$

with x the direction normal to the inlet boundary. From this heat flux, the local mass flux and gas temperature generated by the ingredient regression are computed employing correlations:

$$T_s = f^T(Q) \tag{6}$$

$$\dot{m} = f^M(Q) \tag{7}$$

These dependencies f^T and f^M encapsulate the condensed-phase behaviour and are specific to each ingredient (pure AP, homogenized AP/HTPB, pure RDX). They are obtained numerically, performing coupled 1D simulations as discussed in Section 2.2.2 for various imposed values of Q. The injected gas composition is obtained from condensed-phase decomposition models designed for each ingredient.

4. 2D Numerical Results

The numerical method described in Section 3 is now employed to simulate the heterogeneous combustion of an RDX particle surrounded by a layer of homogenized AP/HTPB binder. The chemical kinetics for the AP/HTPB/RDX system is modelled with the mechanism presented in Section 2.

4.1 Flame Structure

The flame structure forming above such AP/HTPB/RDX composite propellant is first described. The simulated case corresponds to an RDX particle of 400 µm surrounded by a layer of homogenized AP/HTPB binder with 77.5% AP mass loading. The binder layer thickness is chosen to ensure that the overall modelled propellant contains 43% mass fraction of RDX and 43% mass fraction of AP, corresponding to a propellant experimentally studied by Kuwahara et al. [5].

4.1.1 Temperature Field

The computed AP/HTPB/RDX flame is presented in Figure 5a for a pressure of 20 atm. Replacing the RDX particle with an AP particle, the flame for a conventional AP/HTPB propellant is obtained, Figure 5b. This latter flame was previously studied by Gross and Beckstead [3], and acts as a reference to assess the effect of RDX particle combustion.

Introducing RDX particles appears to significantly influence the flame structure forming above the propellant. In the reference case with AP acting as the oxidizer particle, Figure 5b, the well-known Beckstead-Derr-Price (BDP) heterogeneous flame model [29] is recovered. In the BDP model, a premixed zone with a flame temperature around 1400 K is formed above the AP particle, resulting from its combustion in a monopropellant regime. At the AP/binder interface, a primary diffusion flame is found as the gaseous products from pure AP encounter the gases from the homogenized AP/HTPB binder. At the outer radial boundary, far from the AP particle, the homogenized binder burns in a monopropellant regime. A final diffusion flame is located farther from the propellant surface, with high flame temperature around 2800 K.

Considering an RDX particle, Figure 5a, the BDP model does not appear to be applicable any more. For $r < 200$ µm, a high-temperature triangle-shaped flame is standing close to the RDX particle surface. It corresponds to the flame produced by the RDX monopropellant combustion, with a characteristic flame temperature of 3000 K. For $r > 200$ µm above the homogenized AP/HTPB binder, similarly as in the conventional case with an AP particle, the binder combustion produces a premixed flame, with a maximum temperature of 1600 K. A mixing layer is formed at the interface between these two flames, before they merge in a single homogeneous reaction zone far downstream.

To better assess the structure of the flame, the temperature profiles for three radial positions are traced in Figure 6: $r = 0$ µm at the centre of the RDX particle, $r = 200$ µm at the RDX/binder interface, and $r = 279$ µm at the outer edge of the binder. The profile at $r = 0$ µm shows a steep increase up to 3000 K, corresponding to the RDX flame zone with maximum temperature, before decreasing upon mixing with the colder gases produced on the binder side. At the RDX/binder interface, the temperature profile first displays a quick increase in the first few microns before slowing down, owing to the slow-down in RDX-specific reactions caused by the dilution with the gases from the binder. Above the binder, the temperature profile exhibits the characteristic shape of a homogenized AP/HTPB propellant flame, quickly increasing up to 1600 K near the surface before steadily reaching 2000 K during mixing with the hot gases produced by the RDX combustion.

DOI: 10.13009/EUCASS2023-332

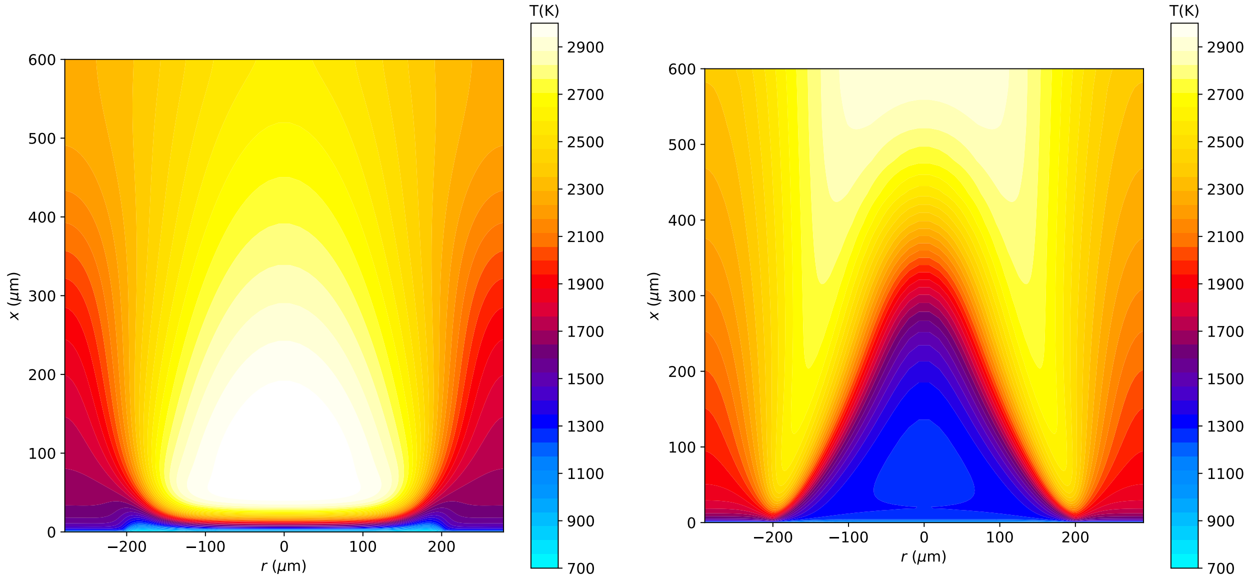

(a) Oxidizer particle: RDX.

(b) Oxidizer particle: AP.

Figure 5: Temperature field in the flame above an oxidizer particle surrounded by a layer of homogenized AP(77.5%)/HTPB binder. Oxidizer particle size 400 µm. Pressure 20 atm.

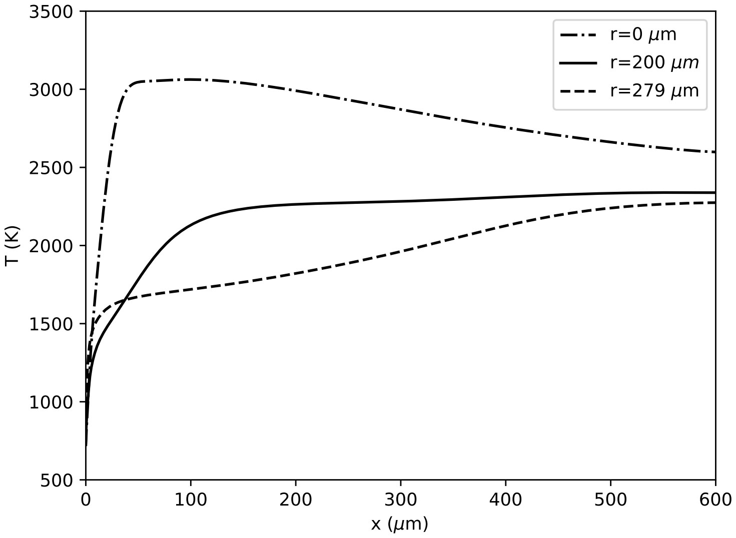

Figure 6: Temperature profiles in the flame above an RDX particle surrounded by a layer of homogenized AP(77.5%)/HTPB binder, for three radial positions. RDX particle size 400 µm. Pressure 20 atm.

Overall, the main difference with respect to the conventional case of AP/HTPB propellant is the absence of any significant diffusion flame caused by mixing of the combustion products from the two ingredients. Each ingredient (RDX and homogenized AP/HTPB binder) appears to burn on its own without significant interaction of their combustion products, before merging into a single flame far downstream when all the gases produced are well mixed. Interactions are limited to a diffusion layer near the RDX/binder interface, where RDX-specific reactions are slowed down due to dilution.

4.1.2 Flame Chemistry

To more finely understand the processes occurring inside the flame and propose a description for its overall structure, it is necessary to study the production and consumption of chemical species. Mass fraction fields are presented in Figure 7 for stable combustion products.

CO is one of the main combustion products: it is produced quickly in the first steps of RDX combustion and is formed later in the mixing zone with binder products. Indeed, binder decomposition forms C_4H_6 molecules which take a long time to be oxidized owing to intermediate isomerisation reactions. Note that CO is mainly formed rather than CO_2 due to the lack of O_2 in the flame: this is a prominent feature of RDX, which is a molecule with a negative oxygen balance ($C_3H_6N_6O_6$). O_2 is formed on the binder side from the homogenized AP and quickly consumed to oxidate C_4H_6 produced by the HTPB pyrolysis. Some O_2 is also formed within the RDX flame, where the temperature is high enough to dissociate the final products. CO_2 appears to be mainly formed near the propellant surface where oxidizing species are still present in significant quantities, before being converted into CO farther in the flame as the oxidizer content drops.

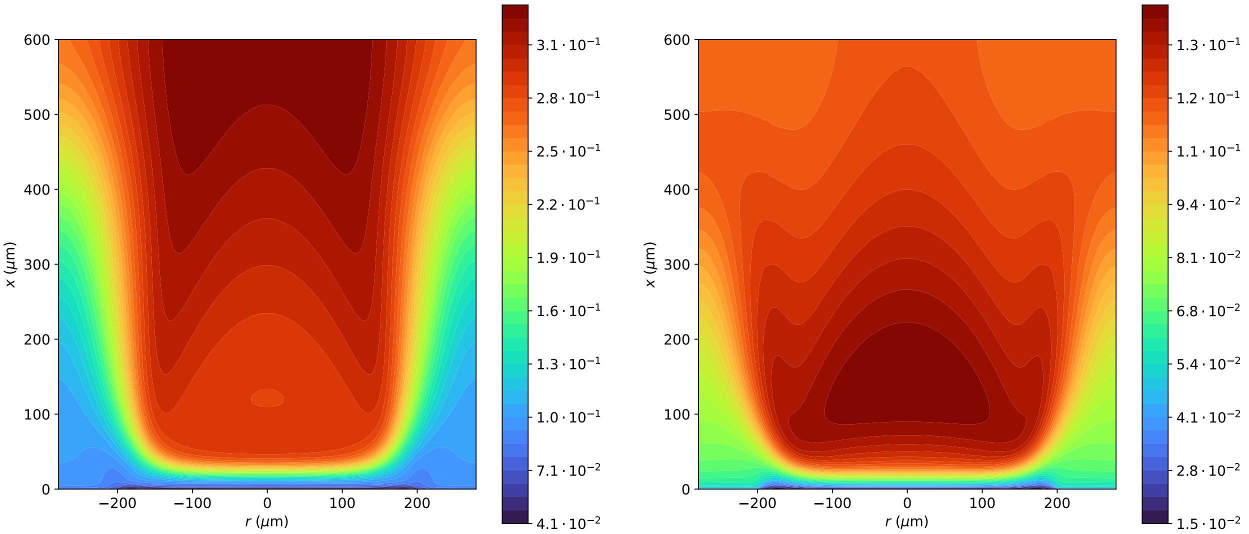

(a) CO.

(b) CO_2.

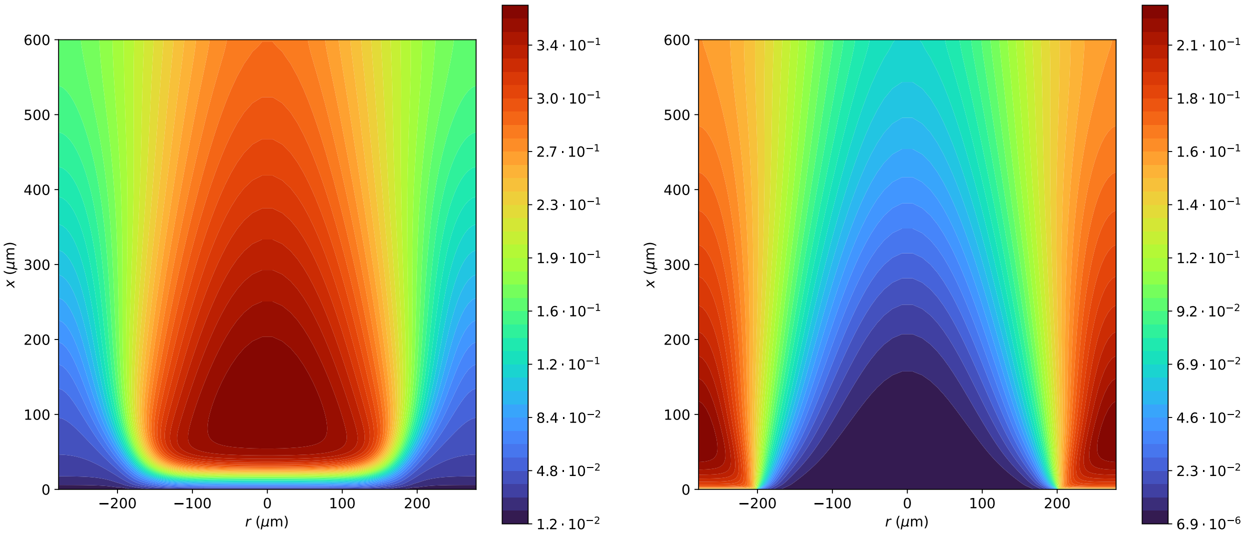

(c) N_2.

(d) HCl.

Figure 7: Major products mass fraction fields in the flame above an RDX particle surrounded by a layer of homogenized AP(77.5%)/HTPB binder. RDX particle size 400 µm. Pressure 20 atm.

The main combustion product of RDX is N_2, which is quickly formed in large quantities near the particle surface. The diffusion effects within the flame are well evidenced by the N_2 and HCl fields far from the propellant surface. HCl is produced by the AP combustion within the homogenized AP/HTPB binder and diffuses toward the centerline. Here, under high temperatures HCl goes through a dissociative reaction to form H and Cl atoms. These H atom react to form H_2 mainly starting 100 µm above the RDX/binder interface. H_2 is formed in larger quantities in the mixing zone above the interface and father from the surface where H_2O produced at the binder side is consumed as oxidizer.

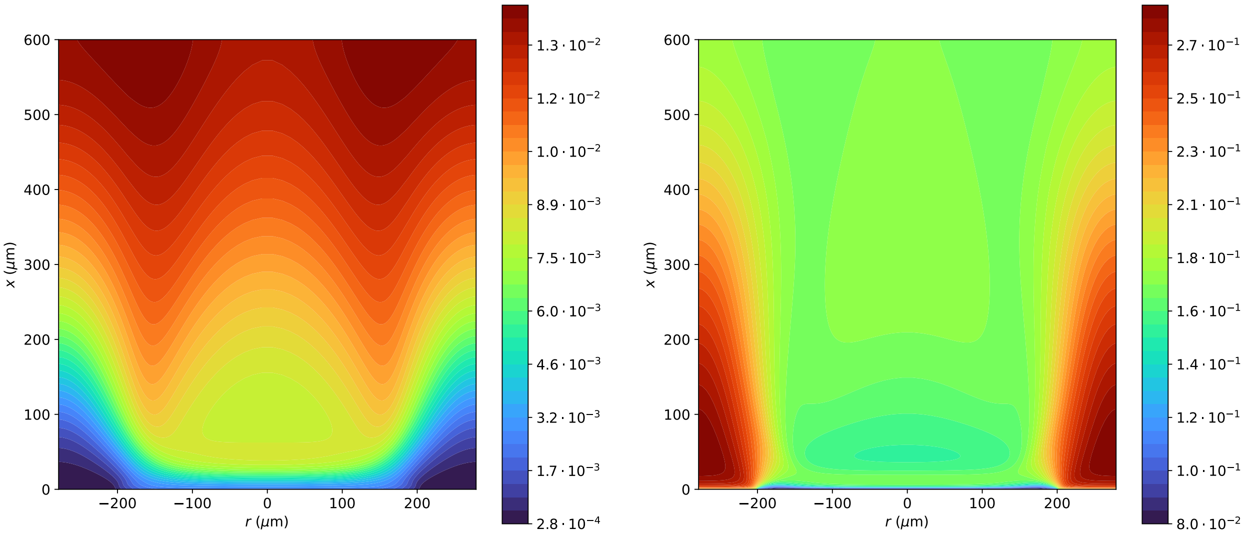

(e) H_2.

(f) H_2O.

Figure 7: Major products mass fraction fields in the flame above an RDX particle surrounded by a layer of homogenized AP(77.5%)/HTPB binder. RDX particle size 400 µm. Pressure 20 atm. (cont.)

Reaction zones can also be characterized by the formation of specific radical species. The mass fraction fields for NO and N radicals are presented in Figure 8. N atom appears to be characteristic of the high-temperature RDX flame. It is formed in large quantities as the temperature approaches its maximum and sufficient energy is available to form this radical. It is then quickly consumed to mainly form the end product N_2, but stays present in areas with sufficiently high temperatures. NO is found mainly close to the particle surface as an intermediate species following the RDX molecule break-down. The NO level quickly drops above the particle central area as NO is consumed by high-temperature reactions to form N_2. The NO fraction remains longer toward the particle edge as the reactions are slowed-down with the temperature reduction in the RDX flame. Note that for this AP/HTPB/RDX propellant, NO is also produced by the combustion of the AP contained in the binder, and acts as an oxidizer in the mixing layer between the RDX and binder flames.

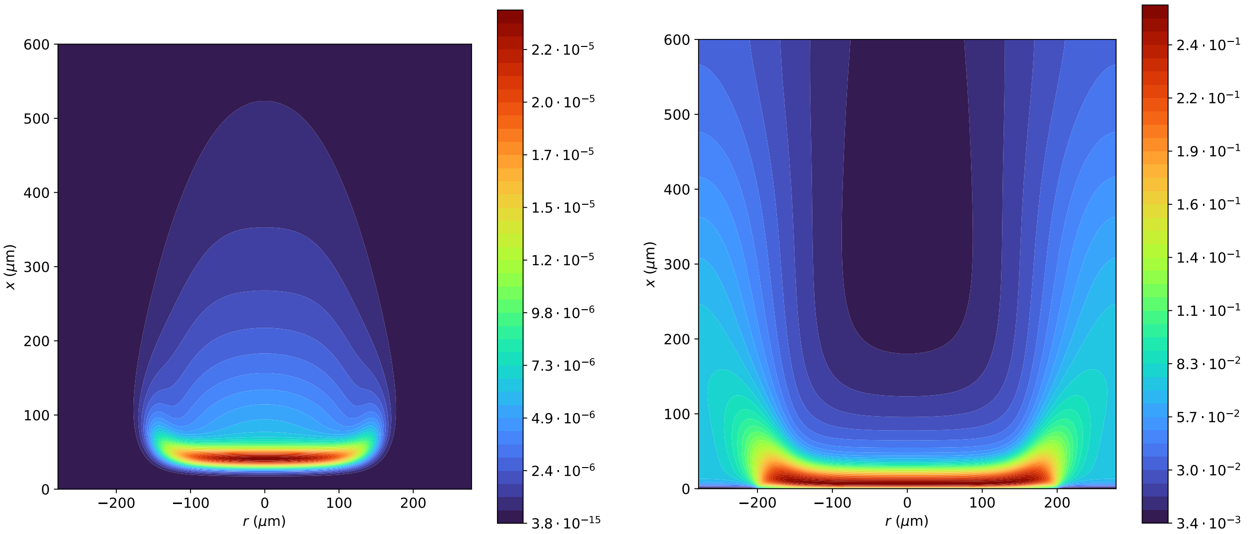

(a) N.

(b) NO.

Figure 8: N and NO mass fraction fields in the flame above an RDX particle surrounded by a layer of homogenized AP(77.5%)/HTPB binder. RDX particle size 400 µm. Pressure 20 atm.

DOI: 10.13009/EUCASS2023-332

4.1.3 Phenomenological Description

To the authors' knowledge, this is the first simulation of the flame structure above such AP/HTPB/RDX propellant. The following phenomenological description is proposed with 4 distinct reaction zones:

- High-temperature RDX flame. Located above the RDX particle, it results mainly from reactions associated with RDX monopropellant combustion, even though species from the binder side can diffuse and react within it, such as HCl forming Cl and H. It is characterized by high temperatures up to 3000 K and the formation of specific radical species such as N atoms.
- Binder premixed flame. This flame is produced above the homogenized AP/HTPB binder, resulting from its combustion in the monopropellant regime. The temperature is around 1600 K. It is characterized by the highest concentration of H_2O and the presence of hydrocarbon species formed at different stages of C_4H_6 oxidation.
- Diffusion layer. Located between the RDX and binder flames, it is primarily distinguished by gradual variations of the gas state parameters across the flow. It is shifted toward the outer boundary due to the hot product expansion in the RDX flame. Specific processes occur within it, as the nitrogen-containing intermediates from the edge of the RDX flame, mainly NO, mix with binder products. Farther from the surface, larger hydrocarbon species are converted into C_2H_2 and partially oxidized consuming H_2O and NO, whereas the temperature increases to 1900 K.
- Final homogeneous flame. Found far downstream, where all the gases mixed by diffusion tend to the equilibrium state. CO and H_2 are mainly produced in this zone from the C_2H_2 conversion process involving H_2O as oxidizer. The temperature tends to 2300 K.

4.2 Effect of Pressure and Particle Diameter

One key feature of composite propellant combustion is their high sensitivity to pressure and oxidizer particle size. For instance, the regression rate of conventional AP/HTPB propellants increases with decreasing particle size, as evidenced by the experimental data in Figure 2b, this effect being more prominent at higher pressure. It is then of practical interest to study the influence of these parameters on the regression of an AP/HTPB/RDX propellant.

4.2.1 Effect of Particle Diameter

With a fixed pressure of 20 atm, the RDX particle diameter is varied from 10 µm to 400 µm, this last RDX size corresponds to the flame described in the previous section, Figure 5a. For each diameter, the computed evolution of the regression rate along the propellant surface is traced in Figure 9.

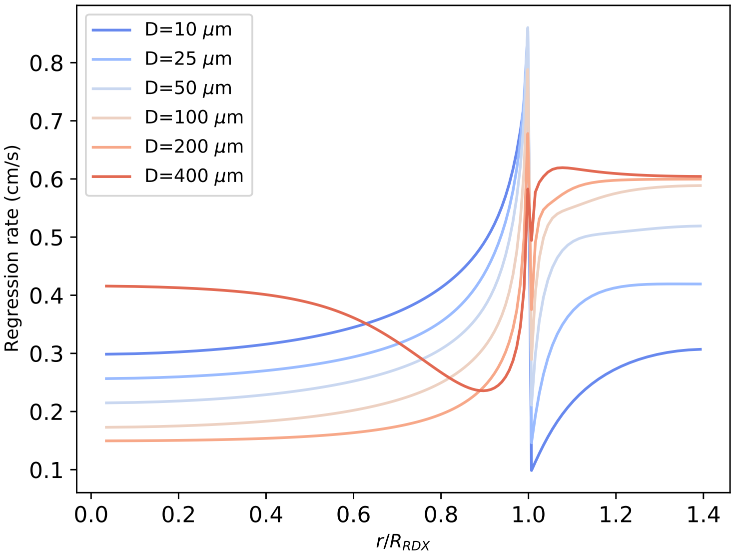

Figure 9: Regression rate of the propellant versus normalized radius for various RDX particle sizes. Homogenized AP(77.5%)/HTPB binder. Pressure 20 atm.

DOI: 10.13009/EUCASS2023-332

RDX particle size has an important effect on the propellant combustion. Above the binder ($r/R_{\mathrm{RDX}} > 1$), the regression rate is maximum for $D_{\mathrm{RDX}} = 400\,\mu\mathrm{m}$. With decreasing particle size, it stays roughly constant at 0.6 cm/s before quickly dropping for particles with diameter $D_{\mathrm{RDX}} < 100\,\mu\mathrm{m}$. Above the RDX particle ($r/R_{\mathrm{RDX}} < 1$) the regression rate is also maximum for $D_{\mathrm{RDX}} = 400\,\mu\mathrm{m}$. However, decreasing the particle size to $D_{\mathrm{RDX}} = 200\,\mu\mathrm{m}$ readily results in a sudden drop in the regression rate before an increase is observed for even smaller particles. This non-monotonous behaviour is peculiar and has not been observed in conventional AP/HTPB propellants.

To better understand this phenomenon, it is helpful to look at the flames obtained for $D_{\mathrm{RDX}} = 200\,\mu\mathrm{m}$ and $D_{\mathrm{RDX}} = 10\,\mu\mathrm{m}$. For $D_{\mathrm{RDX}} = 200\,\mu\mathrm{m}$, the regression rate is strongly reduced for the RDX particle while it stays constant for the binder. For $D_{\mathrm{RDX}} = 10\,\mu\mathrm{m}$, the regression rate for the RDX particle increases while it decreases for the binder. Temperature fields for both flames are shown in Figure 10. The two flames largely differ from the case with $D_{\mathrm{RDX}} = 400\,\mu\mathrm{m}$, previously shown in Figure 5a.

For $D_{\mathrm{RDX}} = 200\,\mu\mathrm{m}$, the high-temperature RDX flame is no longer observed. The field is almost homogeneous at $x > 200\,\mu\mathrm{m}$ with the temperature level typical for the dark zone usually observed in the case of laser-assisted RDX combustion [12]. The combustion process within this zone produces primarily H_2O and nitrogen-containing intermediates (mainly HCN and NO), whereas H_2, CO, and CO_2 are only partially formed. In the absence of intense combustion near the RDX surface, the x-wise temperature gradient and, consequently, the surface heat flux decreases, explaining the sudden drop in the regression rate. The reason for the high-temperature flame disappearance is the strong sensitivity to temperature and dilution of reactions involved in the conversion of the nitrogen-containing intermediates into the final products (N_2, CO, and CO_2) producing the major heat release. Decreasing the particle size enhances the diffusion and heat transfer effects across the flow, thus inducing an inhibiting effect on the high-temperature combustion.
On the other hand, the binder premixed flame does not appear to be influenced, hence the regression rate on the binder side is almost unchanged.

For $D_{\mathrm{RDX}} = 10\,\mu\mathrm{m}$, the diffusion and heat transfer across the flow are even more important, so the flame on the binder side is also affected by slowing down the temperature rise near the surface and hence the regression rate. On the other hand, the same factors promote reactions near the RDX surface by accelerating its regression. In particular, the O_2 diffusion from the binder to the RDX surface is one of such promotive factors.

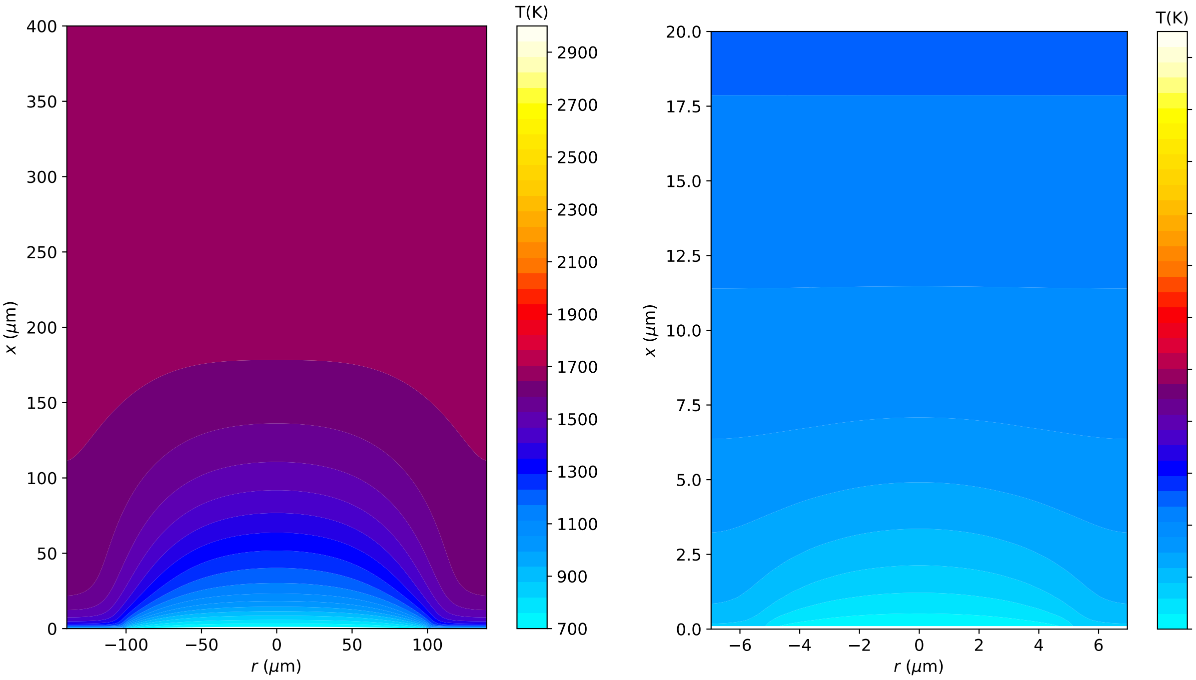

(a) $D_{\mathrm{RDX}} = 200\,\mu\mathrm{m}$.

(b) $D_{\mathrm{RDX}} = 10\,\mu\mathrm{m}$.

Figure 10: Effect of the RDX particle diameter on the flame temperature for the AP/HTPB/RDX propellant. Homogenized AP(77.5%)/HTPB binder. Pressure 20 atm.

DOI: 10.13009/EUCASS2023-332

Overall, the effect of RDX particle diameter can be summarized as follow:

- For a given pressure P, it exists a critical RDX particle diameter noted $D^{\blacklozenge}(P)$. For $D_{\mathrm{RDX}} \geq D^{\blacklozenge}(P)$, a high-temperature flame is attached to the RDX particle, and the propellant burns in a "hot combustion mode".
- For $D_{\mathrm{RDX}} \leq D^{\blacklozenge}(P)$, the high-temperature flame is extinguished due to dilution and heat-loss effects, causing reduction in the RDX regression rate. The propellant burns in a "mild combustion mode". Two regimes may be obtained in this mode. In the first one, the RDX combustion is slow and controlled by the "dark flame" mechanism, but without significant effect on the premixed flame and surface regression on the binder side. The second regime takes place at sufficiently small D_{RDX} when the binder regression rate reduces and the combustion processes above both ingredients are mutually affected, forming a nearly homogeneous flame.

4.2.2 Effect of Pressure

Pressure is known to also influence the combustion of composite propellants. To study its effect, simulations are performed over a wide range of pressures for two fixed RDX particle sizes, $D_{\mathrm{RDX}} = 100\,\mu\mathrm{m}$ and $200\,\mu\mathrm{m}$. We define the mean regression rate of the propellant as:

$$\overline{V}_{\mathrm{reg}} = \frac{2}{R^2}\int_0^R V_{\mathrm{reg}}\, r dr \tag{8}$$

Where R is the radius of the simulation domain and V_{reg} is the local regression rate. The mean regression rate obtained for the two chosen diameters is traced versus pressure in Figure 11.

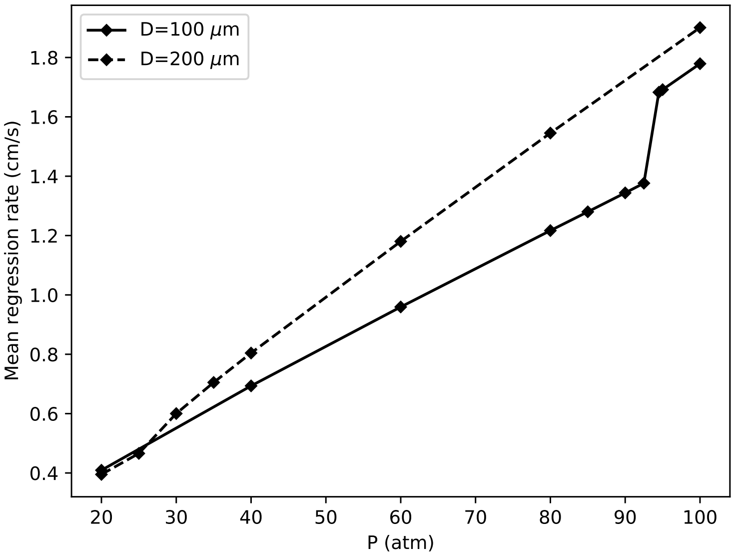

Figure 11: Mean regression rate versus pressure for two RDX particle diameters.

For both particle diameters, the mean regression rate is similar for $P < 25$ atm. Above this pressure, the slope of the $D_{\mathrm{RDX}} = 200\,\mu\mathrm{m}$ curve increases, while it stays constant for $D_{\mathrm{RDX}} = 100\,\mu\mathrm{m}$. At a higher pressure of 94 atm, the $D_{\mathrm{RDX}} = 100\,\mu\mathrm{m}$ curve exhibits, in turn, a break and a sudden increase in its slope. The slope changes observed for both diameters are caused by the combustion mode transition from mild to hot. An important feature is that the change in the combustion mode occurs at a higher pressure for the propellant with smaller RDX particles.

The flame transition from the mild to hot mode is shown in Figure 12 for the particle size $D_{\mathrm{RDX}} = 100\,\mu\mathrm{m}$.
For $P = 94.5$ atm, the hot combustion mode is obtained. The four flame zones, identified in Section 4.1.3, are well present. A high-temperature flame is attached to the RDX particle. The binder produces a premixed flame, both flames being separated by a mixing layer. A homogeneous final zone is formed farther downstream, for $x > 250\,\mu\mathrm{m}$.
On the other hand, the mild combustion mode is obtained for the slightly lower pressure $P = 92.5$ atm. The RDX flame becomes much less intense whereas the binder flame is slightly affected. At the domain centreline, the temperature approaches 2000 K at $x = 50\,\mu\mathrm{m}$ and remains almost constant up to $x = 250\,\mu\mathrm{m}$, then it slowly grows to the final level of 2250 K in the homogeneous zone. Due to dilution and heat losses caused by diffusive effects and insufficient pressure, reactions specific to the high-temperature flame are slowed down or suppressed, so that they cannot produce a second flame front as in the case of laser-assisted RDX combustion [12]. With increased pressure these reactions progress faster, producing more heat which helps establish a high-temperature flame.

DOI: 10.13009/EUCASS2023-332

Overall, the effect of pressure can be summarized as follows:

- For each RDX particle diameter D_{RDX}, there exists a critical pressure $P^{\blacklozenge}(D_{\mathrm{RDX}})$, passed by which the combustion mode changes from mild to hot. Note that it is simply the counterpart of the critical diameter $D^{\blacklozenge}(P)$ evidenced in the previous section.
- This critical pressure increases with decreasing RDX particle size: obtaining hot combustion mode with small RDX particles requires high pressures.

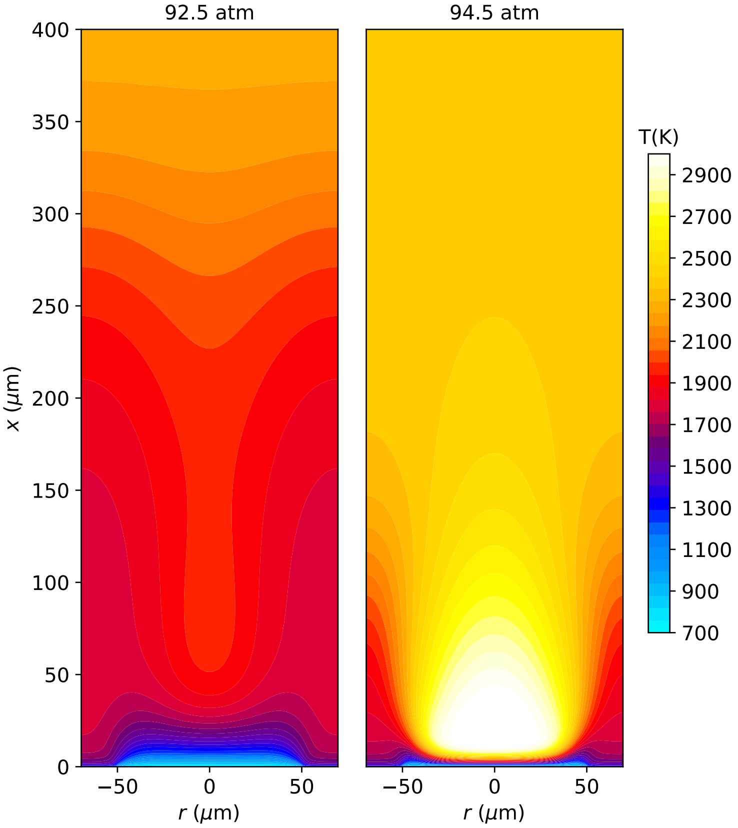

Figure 12: Transition form the mild to hot combustion mode for the AP/HTPB/RDX propellant caused by an increase in pressure from 92.5 to 94.5 atm. RDX particle size 100 µm. Homogenized AP(77.5%)/HTPB binder.

4.2.3 Summary

It is shown by modelling approach that AP/HTPB/RDX propellants can have two combustion modes: the hot one with a high-temperature RDX flame and the mild mode resulting from a slow-down of RDX-specific reactions at the propellant surface. This slow-down is caused by exchanges between the RDX flame and colder gases formed at the binder side, resulting in dilution and heat losses.

The combustion regime is strongly influenced by the ambient pressure and RDX particle size through the diffusion effects. Hot combustion mode is obtained for a combination of sufficiently high pressure and large enough RDX particles: increasing the RDX particle size reduces its relative perimeter and enlarges the distance the gases produced by each ingredient must travel before mixing. On the other hand, increasing the pressure decreases the mean free path for molecular diffusion. Therefore, high pressures and large RDX particles limit interactions between the RDX and binder flames and result in faster and stable propellant regression.

Note that this behaviour is the opposite of what is usually observed for conventional AP/HTPB propellants. It is well-known that for these formulations a reduction in the AP particle size leads to an increase in the overall regression rate. On the other hand, for AP/HTPB/RDX propellant, use of large RDX particles should be preferred to obtain a stable combustion regime.

DOI: 10.13009/EUCASS2023-332

5. Concluding Remarks

The effect of RDX particle inclusion in an AP/HTPB composite propellant has been studied.

A detailed combustion model for the AP/HTPB/RDX system has been developed to simulate the heterogeneous combustion of such propellant. It is built upon previous work on pure AP combustion [6] and is validated against available data for the three ingredients (pure AP, homogenized AP/HTPB, pure RDX).

The μSCOP code has been presented, dedicated to the simulation of the heterogeneous combustion of composite propellants, following the method employed by Gross and Beckstead [3] in their similar study on conventional AP/HTPB propellants.

Following these two preliminary works, the flame structure forming above an RDX particle surrounded by a layer of homogenized AP/HTPB binder has been simulated employing detailed kinetics, for which a phenomenological description has been proposed. The effect of RDX particle diameter and pressure on the combustion has been highlighted. The main results obtained can be summarized as follows:

- AP/HTPB/RDX propellants can burn following two distinct combustion modes: mild and hot.
- In the hot combustion mode, a high-temperature flame is attached to the RDX particle surface. This mode provides the maximum regression rate for the propellant and is achieved at sufficiently high pressure and large RDX particle size.
- In the mild combustion mode, the RDX flame temperature is strongly decreased, reducing the overall regression rate of the propellant. Dilution and heat exchange with binder gases close to the surface slow down RDX-specific reactions. This mode is obtained by reducing pressure or RDX particle size below critical values.

To the knowledge of the authors, this is the first numerical study of this kind. The main takeaway is the negative impact of RDX particle size reduction on the regression rate of AP/HTPB/RDX propellants, as opposed to the positive effect of AP particle size reduction observed for conventional AP/HTPB propellant. Further work might be needed to confirm these numerical findings. Interactions between the gases from burning RDX and AP are not well understood, and it is possible that some reactions between them might be missing. Experimental work involving AP/RDX sandwich propellant could provide some insight into this matter. Furthermore, experimental data on AP/HTPB/RDX is quite rare. Work could be dedicated to visualisation of the flame structure for such propellants.

6. Acknowledgments

The authors would like to thank the French Defense Innovation Agency (AID), the French Procurement Agency for Armament (DGA) and the ONERA for funding and supporting the present work.

References

[1] O. Korobeinichev, A. Chernov, I. Emel'Yanov, N. Ermolin, and T. Trofimycheva, "Investigation of the kinetics and the chemical reaction mechanism in the flame of a mixed compound, based on ammonium perchlorate and polybutadiene rubber," *Combust. Explo. Shock.*, vol. 26, pp. 292–300, 1990.

[2] M. Jeppson, M. Beckstead, and Q. Jing, *A kinetic model for the premixed combustion of a fine AP/HTPB composite propellant*. 36th AIAA Aerospace Sciences Meeting and Exhibit, 1998.

[3] M. Gross and M. Beckstead, "Diffusion flame calculations for composite propellants predicting particle-size effects," *Combust. Flame*, vol. 157, pp. 864–873, 2010.

[4] N. Kubota, "Combustion mechanisms of nitramine composite propellants," in *Symposium (International) on Combustion*, vol. 18, pp. 187–194, 1981.

[5] T. Kuwahara and N. Kubota, "Combustion of RDX/AP composite propellants at low pressures," *J. Spacecraft. Rockets.*, vol. 21, pp. 502–507, 1984.

[6] P. Bernigaud, D. Davidenko, and L. Catoire, "A revised model of ammonium perchlorate combustion with detailed kinetics," *Combust. Flame*, Accepted, 2023.

[7] N. Ermolin, "Model for chemical reaction kinetics in perchloric acid-ammonia flames," *Combust., Explo. Shock.*, vol. 31, pp. 555–565, 1995.

DOI: 10.13009/EUCASS2023-332

[8] N. Meynet, *Simulation numérique de la combustion d'un propergol solide*. PhD thesis, Université Paris VI, 2005.

[9] K. Shrestha, L. Seidel, T. Zeuch, and F. Mauss, "Detailed kinetic mechanism for the oxidation of ammonia including the formation and reduction of nitrogen oxides," *Energ. Fuel.*, vol. 32, pp. 10202–10217, 2018.

[10] A. Laskin, H. Wang, and C. Law, "Detailed kinetic modeling of 1, 3-butadiene oxidation at high temperatures," *Int. J. Chem. Kinet.*, vol. 32, pp. 589–614, 2000.

[11] M. Pelucchi, A. Frassoldati, T. Faravelli, B. Ruscic, and P. Glarborg, "High-temperature chemistry of HCl and Cl2," *Combust. Flame*, vol. 162, pp. 2693–2704, 2015.

[12] K. Prasad, R. Yetter, and M. Smooke, "An eigenvalue method for computing the burning rates of RDX propellants," *Combust. Sci. Technol.*, vol. 124, pp. 35–82, 1997.

[13] S. Rahman, V. Giovangigli, and V. Borie, "Pressure and initial temperature sensitivity coefficient calculations in ammonium perchlorate flames," *J. Propul. Power*, vol. 27, pp. 1054–1063, 2011.

[14] T. Boggs, "Deflagration rate, surface structure, and subsurface profile of self-deflagrating single crystals of ammonium perchlorate," *AIAA J.*, vol. 8, pp. 867–873, 1970.

[15] A. Atwood, T. Boggs, P. Curran, T. Parr, D. Hanson-Parr, C. Price, and J. Wiknich, "Burning rate of solid propellant ingredients, part 1: Pressure and initial temperature effects," *J. Propul. Power*, vol. 15, pp. 740–747, 1999.

[16] D. A. Smyth, *Modeling Solid Propellant Ignition Events*. PhD thesis, Brigham Young University, 2011.

[17] E. Cohen-Nir, "Temperature sensitivity of the burning rate of composite solid propellants," *Combust. Sci. Technol.*, vol. 9, pp. 183–194, 1974.

[18] R. Foster, J. Condon, and R. Miller, "Low exponent technology," *Hercules Report, AFRPL-TR-81*, vol. 95, 1982.

[19] R. Bellec, J. Duterque, and G. Lengelle, "Modeling of aluminized solid propellants," *ONERA, Technical Report RT 37/7128 EN*, 1996.

[20] A. Zenin, "HMX and RDX-combustion mechanism and influence on modern double-base propellant combustion," *J. Propul. Power.*, vol. 11, pp. 752–758, 1995.

[21] A. Atwood, P. Curran, and C. Price, "Laboratory ignition and combustion data and the determination of global kinetics and energetic parameters of rdx," in *Proceedings of the 32nd JANNAF Combustion Subcommittee Meeting*, 1995.

[22] A. Ulas, Y.-C. Lu, and K. Kuo, "Ignition and combustion characteristics of RDX-based pseudopropellants," *Combust. Sci. Technol.*, vol. 175, pp. 695–720, 2003.

[23] A. Glazkova, "The effect of catalysts on the combustion of explosives," *Combust., Explo. Shock.*, vol. 10, pp. 281–290, 1974.

[24] E. Volkov, A. Paletsky, and O. Korobeinichev, "RDX flame structure at atmospheric pressure," *Combust., Explo. Shock.*, vol. 44, pp. 43–54, 2008.

[25] A. Ern and V. Giovangigli, "Fast and Accurate Multicomponent Transport Property Evaluation," *J. Comput. Phys.*, vol. 120, pp. 105–116, Aug. 1995.

[26] R. Kee, F. Rupley, E. Meeks, and J. Miller, "Chemkin-II: A FORTRAN chemical kinetics package for the analysis of gas-phase chemical and plasma kinetics," *Sandia National Laboratories, Technical Report SAND-89-8009*, 1989.

[27] D. Kim and H. Choi, "A second-order time-accurate finite volume method for unsteady incompressible flow on hybrid unstructured grids," *J. Comput. Phys.*, vol. 162, pp. 411–428, 08 2000.

[28] S. Abhyankar, J. Brown, E. Constantinescu, D. Ghosh, B. Smith, and H. Zhang, "PETSc/TS: A modern scalable ODE/DAE solver library," *arXiv preprint arXiv:1806.01437*, 2018.

[29] M. Beckstead, R. Derr, and C. Price, "A model of composite solid-propellant combustion based on multiple flames," *AIAA J.*, vol. 8, pp. 2200–2207, 1970.